Origin of Thermal Degradation of Sr$_{2-x}$Si$_5$N$_8$:Eu$_x$ Phosphors in Air for Light-Emitting Diodes

Chiao-Wen Yeh,[†] Wei-Ting Chen,[†] Ru-Shi Liu,*,[†] Shu-Fen Hu,[‡] Hwo-Shuenn Sheu,[§] Jin-Ming Chen,[§] and Hubertus T. Hintzen[‖]

[†]Department of Chemistry, National Taiwan University, Taipei 106, Taiwan
[‡]Department of Physics, National Taiwan Normal University, Taipei 116, Taiwan
[§]National Synchrotron Radiation Research Center, Hsinchu 300, Taiwan
[‖]Laboratory of Energy Materials and Devices, Eindhoven University of Technology, P.O. Box 513, 5600 MB Eindhoven, The Netherlands

ABSTRACT: The orange-red emitting phosphors based on M$_2$Si$_5$N$_8$:Eu (M = Sr, Ba) are widely utilized in white light-emitting diodes (WLEDs) because of their improvement of the color rendering index (CRI), which is brilliant for warm white light emission. Nitride-based phosphors are adopted in high-performance applications because of their excellent thermal and chemical stabilities. A series of nitridosilicate phosphor compounds, M$_{2-x}$Si$_5$N$_8$:Eu$_x$ (M = Sr, Ba), were prepared by solid-state reaction. The thermal degradation in air was only observed in Sr$_{2-x}$Si$_5$N$_8$:Eu$_x$ with x = 0.10, but it did not appear in Sr$_{2-x}$Si$_5$N$_8$:Eu$_x$ with x = 0.02 and Ba analogue with x = 0.10. This is an unprecedented investigation to study this phenomenon in the stable nitrides. The crystal structural variation upon heating treatment of these compounds was carried out using the in situ XRD measurements. The valence of Eu ions in these compounds was determined by electron spectroscopy for chemical analysis (ESCA) and X-ray absorption near-edge structure (XANES) spectroscopy. The morphology of these materials was examined by transmission electron microscopy (TEM). Combining all results, it is concluded that the origin of the thermal degradation in Sr$_{2-x}$Si$_5$N$_8$:Eu$_x$ with x = 0.10 is due to the formation of an amorphous layer on the surface of the nitride phosphor grain during oxidative heating treatment, which results in the oxidation of Eu ions from divalent to trivalent. This study provides a new perspective for the impact of the degradation problem as a consequence of heating processes in luminescent materials.
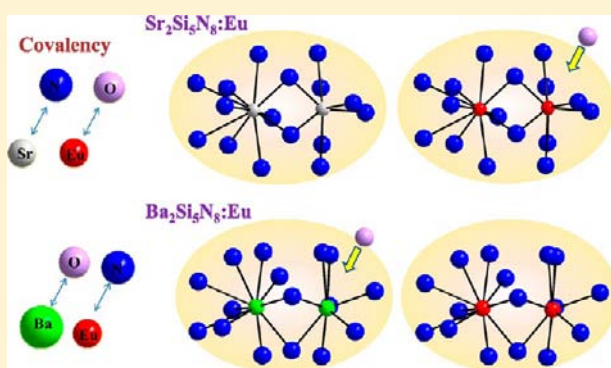
INTRODUCTION

Recently, white light-emitting diodes (WLEDs), which are regarded as the next-generation lighting sources, have been used as backlight, flashlight, automobile headlamp, etc. They have a tendency to replace the conventional incandescent and fluorescent lamps because of their high energy efficiency, durability, reliability, and capability to be used in products with various sizes and eco-friendly components.[1] Generally, the main modus for producing white LEDs is the phosphor conversion method. The phosphors are composed of a host lattice and a small amount of activators as the luminescence centers. Down conversion luminescent materials used in LEDs convert the emission from ultraviolet (UV) or blue chip to longer wavelength light by using phosphors. The most widely adopted white light LED is a combination of an InGaN device with 460 nm blue light and YAG:Ce (Y$_3$Al$_5$O$_{12}$:Ce) phosphor, which emits yellow light. However, the color-rendering index of such a white light LED is poor.[2] Warm white light illumination could not be achieved by this approach because of the shortage of long-wavelength spectral emission in such LEDs. In the past

few years, nitridosilicates and oxonitridosilicates have been utilized in structural ceramics and advanced optical materials, because of their exceptional chemical and physical stabilities. Rare-earth doped nitridosilicates and oxonitridosilicates exhibit long wavelength emissions, which are attributed to high covalence of the host-lattice and a large crystal field splitting effect of the Eu^{2+} 5d band associated with the presence of coordinated nitrogen.[3] It provides a superior high color rendering index (Ra) when combining with blue and green emission, resulting in color uniformity and excellent quality of emission. Among numerous candidate (oxo)nitridosilicates phosphors, MSi$_2$O$_2$N$_2$ (M = Ca, Sr, Ba), M$_2$Si$_5$N$_8$ (M = Ca, Sr, Ba), and MAlSiN$_3$ (M = Ca, Sr) are suitable host lattices for highly efficient rare-earth doped luminescent materials in WLEDs applications.[4]

In 1999, (Ca,Sr,Ba)$_{2-x}$Si$_5$N$_8$:Eu$_x$ was patented as a red emitting component in phosphor-conversion LEDs (pc-LEDs)

because it could be brought up to full spectrum of lighting.[5] These phosphors are synthesized under ambient pressure and have a lower cost in production than high-pressure synthesis of luminescent materials. The present research in the nitride host lattices $M_2Si_5N_8$ and $MSi_2O_2N_2$ focuses on the development of an appropriate host and the partial replacement of constituents to adjust the emission and excitation wavelengths of the phosphor. However, only 15−20% of the input power to high-power LEDs is output as emitted light. The other 80−85% of the power of LEDs is converted to heat.[6] The consumption of energy therefore heats the device until about 150 °C. The luminescence properties of a phosphor at temperatures above room temperature have been investigated, and the conversion efficiency is declined.[7] Moreover, for a sample with a high concentration of Eu^{2+} dopant, the emission peak is red-shifted, and the intensity decreases more quickly as the temperature is increased.

Relevant literature has discussed the mechanism of thermal quenching in many nitrides; however, thermal degradation has not been discussed in detailed yet.[8] The purpose of this study is to elucidate the thermal degradation of the luminescence in nitridosilicate phosphors, $M_2Si_5N_8$:Eu (M = Sr, Ba).

■ EXPERIMENTAL SECTION

Materials and Synthesis. A series of nitridosilicate phosphors compounds, $M_{2−x}Si_5N_8$:Eu$_x$ (M = Sr, Ba), were prepared by solid-state reactions. Stoichiometric amounts of powdered Sr_3N_2 (Cerac, 99.5%, ∼60 mesh), Ba_3N_2 (Cerac, 99.7%, ∼20 mesh), Si_3N_4 (Aldrich, 99.9%), and EuN (Cerac, 99.9%, ∼60 mesh) were ground in an agate mortar for 30 min in a glovebox to form a homogeneous mixture. The concentrations of both moisture and oxygen in the glovebox are <1 ppm. The mixtures were placed in covered molybdenum crucibles and fired at 1400 °C for 16 h under flowing 90% N_2−10% H_2 atmosphere in a tube furnace. The sintered products were ground again, yielding crystalline powder.

Characterization. All measurements were made on finely ground powder. The phase purity of samples were analyzed by X-ray diffraction (XRD) using a a D2 Phaser (Bruker) diffractometer operated with Cu Kα radiation (λ = 1.5418 Å). The data were gathered over a 2θ range from 10° to 90° at intervals of 0.02° with a counting time of one minute per degree. Rietveld refinements of the X-ray diffractograms were conducted using the GSAS (General Structure Analysis System) program.[9] Photoluminescence (PL) spectra were measured at room temperature using FluoroMax-3 and FluoroMax-P spectrophotometers. Temperature-dependent luminescence (25−300 °C) was conducted using a heating apparatus (THMS-600) in combination with PL equipment. Electron spectroscopy for chemical analysis (ESCA) spectra of the samples was obtained using an ESCA system (VG Scientific ESCALAB 250) with an Al Kα X-ray source. The Eu L_3-edge X-ray absorption near-edge structure (XANES) spectrum was recorded in transmission mode for a sample mounted on Scotch tape at BL17C beamline of the National Synchrotron Radiation Research Center (NSRRC). The incident (I_0) and transmitted (I) beam intensities were measured by the gas-ionization chambers filled with a mixture of N_2 and He gases, and a mixture of N_2 and Ar gases, respectively. The photon energy was calibrated by measuring a simultaneous standard of Fe foils with the known Fe K-edge absorption inflection point at 7112 eV. The high temperature in situ XRD patterns were obtained using a large Debye−Scherrer camera at BL01C2 beamline of the NSRRC with λ = 0.774908 Å. The in situ XRD measurement was performed after 10 min to ensure heat balance. The powder diffraction patterns from synchrotron radiation were converted to the Cu Kα radiation mode for comparison with in-house XRD by WinPLOTR program. Transmission electron microscopic (TEM) micrographs and electron diffraction patterns were obtained on a JEOL JEM-2100F electron microscope.

■ RESULTS AND DISCUSSION

XRD Refinement and Lattice Parameters. The phase purities of the $Sr_{2−x}Si_5N_8$:Eu$_x$ (x = 0.02, 0.10) and $Ba_{2−x}Si_5N_8$:Eu$_x$ (x = 0.10) compounds were confirmed using X-ray powder diffraction (XRD). The Rietveld refinements from XRD patterns indicate that these three compounds exhibit the same crystalline orthorhombic crystal system with a space group $Pmn2_1$. The crystal structures of $Sr_2Si_5N_8$ and $Ba_2Si_5N_8$ from the literature were used as the initial parameters for the Rietveld refinement of the prepared powders.[10] Figure 1 presents the results of the experimental and the calculated X-ray powder diffraction patterns for $Sr_{2−x}Si_5N_8$:Eu$_x$ (x = 0.02, 0.10), $Ba_{2−x}Si_5N_8$:Eu$_x$ (x = 0.10), and the corresponding residuals using the Rietveld refinement. The Eu as isotropic displacement
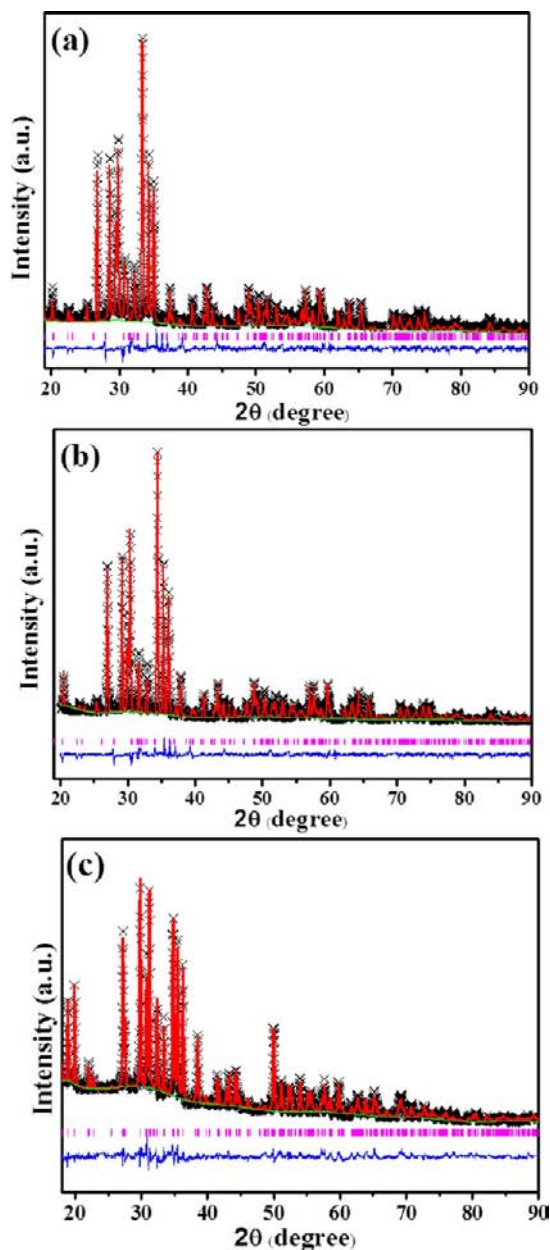

Figure 1. Powder XRD pattern (×) of (a) $Sr_{2−x}Si_5N_8$:Eu$_x$ (x = 0.02), (b) $Sr_{2−x}Si_5N_8$:Eu$_x$ (x = 0.10), and (c) $Ba_{2−x}Si_5N_8$:Eu$_x$ (x = 0.10) samples with their corresponding Rietveld refinement (solid line) and residuals (bottom).

Table 1. Crystallographic Data for $Sr_{2-x}Si_5N_8$:Eu_x ($x = 0.02$), $Sr_{2-x}Si_5N_8$:Eu_x ($x = 0.10$), and $Ba_{2-x}Si_5N_8$:Eu_x ($x = 0.10$) As Determined from Rietveld Refinement

	$Sr_{2-x}Si_5N_8$:Eu_x ($x = 0.02$)	$Sr_{2-x}Si_5N_8$:Eu_x ($x = 0.10$)	$Ba_{2-x}Si_5N_8$:Eu_x ($x = 0.10$)
		Space Group: $Pmn2_1$ (Orthorhombic)	
		Cell Parameter	
a	5.7138 (4) Å	5.7110 (3) Å	5.7789 (2) Å
b	6.8211 (1) Å	6.8299 (4) Å	6.9541 (3) Å
c	9.3363 (4) Å	9.3298 (4) Å	9.3799 (4) Å
$\alpha = \beta = \gamma$	90°	90°	90°
cell volume	364.02 (4) Å³	363.93(1) Å³	376.86 (4) Å³
		Reliability Factors	
R_{wp}	7.76%	5.42%	7.22%
R_p	5.49%	3.92%	5.54%
χ^2	2.83	2.78	3.12

		$Sr_{2-x}Si_5N_8$:Eu_x ($x = 0.02$)			
atom	x	y	z	frac	U_{iso} (Å²)
Sr1	0.00000	0.8652(1)	0.0033(1)	0.99	0.0058(1)
Sr2	0.00000	0.8935(1)	0.3702(3)	0.99	0.0111(2)
Si1	0.2613(1)	0.6561(1)	0.6959(2)	1.00	0.0219(3)
Si2	0.00000	0.0573(2)	0.6677(0)	1.00	0.0111(2)
Si3	0.00000	0.4202(1)	0.4632(1)	1.00	0.0189(1)
Si4	0.00000	0.4047(0)	0.9009(1)	1.00	0.0211(1)
N1	0.00000	0.2186(0)	0.5358(0)	1.00	0.0762(0)
N2	0.2550(1)	0.9043(2)	0.6901(1)	1.00	0.0142(3)
N3	0.2502(1)	0.4647(2)	0.0342(2)	1.00	0.0289(1)
N4	0.00000	0.5935(3)	0.7811(0)	1.00	0.0342(1)
N5	0.00000	0.1757(1)	0.8582(1)	1.00	0.0420(0)
N6	0.00000	0.4253(2)	0.2711(2)	1.00	0.0503(2)
Eu1	0.00000	0.8652(1)	0.0033(1)	0.01	0.0058(1)
Eu2	0.00000	0.8935(1)	0.3702(3)	0.01	0.0111(2)

		$Sr_{2-x}Si_5N_8$:Eu_x ($x = 0.10$)			
atom	x	y	z	frac	U_{iso} (Å²)
Sr1	0.0000	0.8678(0)	−0.0078(1)	0.95	0.0023(2)
Sr2	0.0000	0.8800(1)	0.3595(1)	0.95	0.0072(1)
Si1	0.2531(1)	0.6611(2)	0.6673(1)	1.00	0.0255(0)
Si2	0.0000	0.0598(1)	0.6548(3)	1.00	0.0433(0)
Si3	0.0000	0.4141(0)	0.4479(0)	1.00	0.0221(1)
Si4	0.0000	0.4147(3)	0.8865(2)	1.00	0.0377(3)
N1	0.0000	0.2686(2)	0.4981(3)	1.00	0.0101(1)
N2	0.2433(2)	0.9181(0)	0.6731(2)	1.00	0.0299(2)
N3	0.2528(0)	0.4787(1)	0.0253(1)	1.00	0.0547(0)
N4	0.0000	0.5646(2)	0.7761(0)	1.00	0.0293(2)
N5	0.0000	0.1777(1)	0.8282(5)	1.00	0.0801(3)
N6	0.0000	0.4282(1)	0.2577(2)	1.00	0.0701(1)
Eu1	0.0000	0.8678(1)	−0.0078(1)	0.05	0.0023(1)
Eu2	0.0000	0.8800(1)	0.3595(0)	0.05	0.0072(3)

		$Ba_{2-x}Si_5N_8$:Eu_x ($x = 0.10$)			
atom	x	y	z	frac	U_{iso} (Å²)
Ba1	0.0000	0.8513(0)	−0.0035(0)	0.95	0.0050(1)
Ba2	0.0000	0.8748(2)	0.6428(1)	0.95	0.0083(0)
Si1	0.2521(1)	0.6488(0)	0.3381(1)	1.00	0.0340(1)
Si2	0.0000	0.0562(1)	0.3474(0)	1.00	0.0347(2)
Si3	0.0000	0.4023(1)	0.5603(2)	1.00	0.0663(0)
Si4	0.0000	0.4169(0)	0.1352(1)	1.00	0.0427(1)
N1	0.0000	0.1895(1)	0.4461(1)	1.00	0.0583(1)
N2	0.2690(1)	0.7982(0)	0.2946(0)	1.00	0.0216(1)
N3	0.2768(1)	0.4579(0)	0.9923(2)	1.00	0.0243(3)
N4	0.0000	0.4760(3)	0.1991(1)	1.00	0.0327(1)
N5	0.0000	0.6672(0)	0.7097(1)	1.00	0.0825(0)
N6	0.0000	0.6661(1)	0.8663(3)	1.00	0.0901(1)
Eu1	0.0000	0.8513(0)	−0.0035(0)	0.05	0.0050(1)

Table 1. continued

		$Ba_{2-x}Si_5N_8$:Eu_x ($x = 0.10$)			
atom	x	y	z	frac	U_{iso} (Å²)
Eu2	0.0000	0.8748(2)	0.6428(1)	0.05	0.0083(0)

factors for Sr/Ba atoms in $M_{2-x}Si_5N_8$:Eu_x (M = Sr or Ba) were constrained to be equal, and the metal site occupancies were fixed. The XRD patterns of Eu-doped $M_2Si_5N_8$ (M = Sr, Ba) obtained herein are identical to those published for the single crystals,[11] indicating that single phases are formed without impurities. Additionally, the Rietveld refinement results demonstrate that the both $Sr_2Si_5N_8$ and $Ba_2Si_5N_8$ show pure phase. The detailed crystallographic data are listed in Table 1. The Eu^{2+} dopants replace two Sr^{2+} sites because the ionic radii of Sr^{2+} (r^8 and r^9 are 1.26 and 1.31 Å, respectively) differ slightly from Eu^{2+} (r^8 and r^9 are 1.25 and 1.30 Å, respectively).[11] On the other hand, Eu^{2+} dopants replace two Ba^{2+} sites, because the ionic radii of Ba^{2+} (r^8 and r^9 are 1.42 and 1.47 Å, respectively) are close to those of Eu^{2+} (r^8 and r^9 are 1.25 and 1.30 Å, respectively). According to Vegard's law, the lattice constants and cell volume decrease when the ionic radius of the dopants (Eu) decreases in $M_{2-x}Si_5N_8$:Eu_x (M = Sr or Ba).[12]

On the basis of the results of Rietveld refinement (Figure 1), the structure of $M_2Si_5N_8$ (M = Sr, Ba) has a typical corner-sharing structure. The crystal structure is established from a network of vertex-sharing [SiN₄] tetrahedra that connect two (N[2]) and three (N[3]) neighboring Si atoms. As shown in Figure 2a, perpendicular to the [100] direction, the *sechser* ring
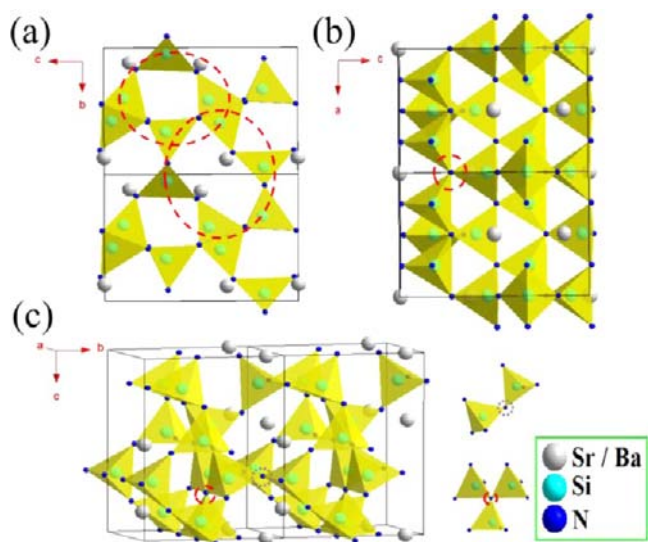

Figure 2. Crystal structures of $M_2Si_5N_8$. The view of the $M_2Si_5N_8$ (M = Sr, Ba) (a) perpendicular to the [100] direction, (b) along the [010] direction, and the (c) corner-sharing SiN₄ tetrahedra three-dimensional network structure.

is formed by the [Si₆N₆] unit, and the *vierer* ring is formed by connection of four tetrahedral units. Therefore, the $M_2Si_5N_8$ (M = Sr, Ba) compounds have two coordination sites. In the [010] direction, corrugated layers of highly condensed *dreier* rings with N[3] atoms are observed as shown in Figure 2 (b). The crystal structure of $M_2Si_5N_8$ (M = Sr, Ba) is a three-dimensional network of corner-sharing SiN₄ tetrahedra, in which one-half of the nitrogen atoms N[2] connecting with two

silicon and the other half of the nitrogen atoms connect to three neighboring Si atoms N[3], Figure 2c.[10,13] Nitrogen is involved in a more varied cross-linking structure in nitridosilicates than in classical oxosilicate and forms a rigid and further stable structure.[14]

Photoluminescence Properties. Figure 3 shows the excitation and emission spectra of $Sr_{2-x}Si_5N_8$:Eu_x ($x = 0.02-$
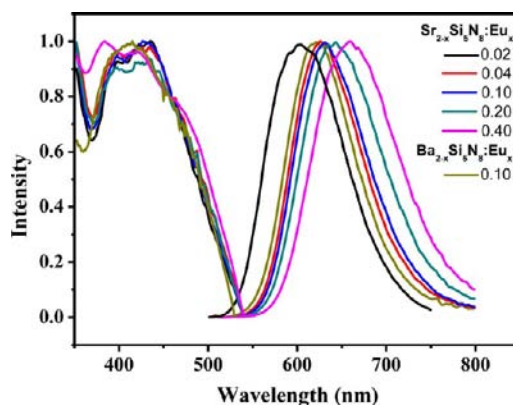

Figure 3. Emission spectra and excitation spectra of $Sr_{2-x}Si_5N_8$:Eu_x with varied content from $x = 0.02$ to 0.40 and $Ba_{2-x}Si_5N_8$:Eu_x ($x = 0.10$).

0.40) and $Ba_{2-x}Si_5N_8$:Eu_x ($x = 0.10$) for comparison. Eu-doped $Sr_{2-x}Si_5N_8$:Eu_x ($x = 0.02-0.40$) exhibits a shift of emission band from 602 to 660 nm with increasing Eu concentration. The excitation spectra in Figure 3 reveal that $Sr_{2-x}Si_5N_8$:Eu_x ($x = 0.02-0.40$) could be excited by UV to blue light. Comparing the emission spectra $Sr_{2-x}Si_5N_8$:Eu_x ($x = 0.10$) and $Ba_{2-x}Si_5N_8$:Eu_x ($x = 0.10$) demonstrates that the emission from the Ba-containing compound is blue-shifted because of the lower crystal field splitting and smaller Stokes shift. The position of the 5d excitation and emission band of the Eu^{2+} ions at lower energy (longer wavelength) is attributed to the influence of highly covalent bonding of Eu−N and high crystal field strength. The length of the Eu−N bonds and the crystal field strength around the Eu^{2+} atom critically affect the emission wavelength. The emission bands associated with different M ions are typical characteristics of Eu-doped alkaline earth silicon nitrides.[15]

Thermal Quenching and Thermal Degradation. A comprehensive understanding of the thermal quenching and thermal degradation of phosphors used in LEDs is indispensable because high-power LEDs suffer from both thermal problems. We have measured temperature-dependent luminescence spectra of $M_2Si_5N_8$ (M = Sr, Ba) in air from 25 to 300 °C and then from 300 to 25 °C, as shown in Figure 4. The emission intensity decreases and the wavelength shifts clearly with increasing temperature, because of nonradiative transitions from the excited state to the ground state. To compare thermal quenching at various Eu concentrations (Figure 4a and b), the interatomic distance between Eu^{2+} ions is shortened with increasing Eu^{2+} concentration, enhancing energy transfer processes. The probability that Eu occupies a lower energy

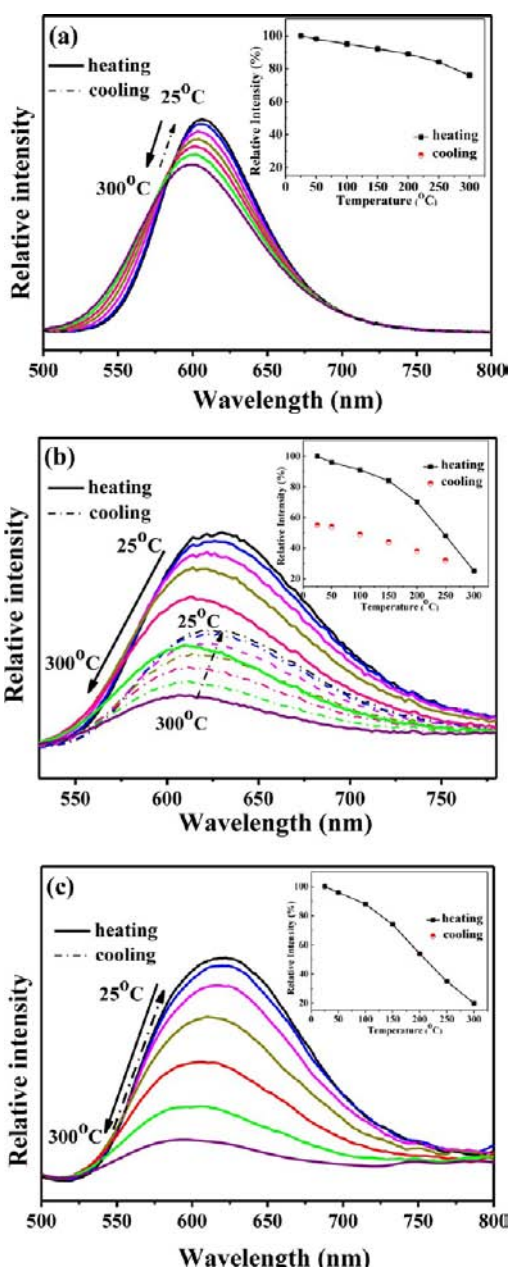**Figure 4.** Temperature dependence of emission spectra of (a) $Sr_{2-x}Si_5N_8$:Eu_x (x = 0.02), (b) $Sr_{2-x}Si_5N_8$:Eu_x (x = 0.10), and (c) $Ba_{2-x}Si_5N_8$:Eu_x (x = 0.10) from 25 to 300 °C (solid line), then cooled from 300 to 25 °C (dash line) under air, with the relative intensity as a function of the temperature plotted in the inset.

level raises with increasing x, leading to a higher relaxation rate in nonradiative transition from excited to ground state. Accordingly, $Ba_{2-x}Si_5N_8$:Eu_x (x = 0.10) shows thermal quenching (Figure 4c), which is somewhat stronger than $Sr_{2-x}Si_5N_8$:Eu_x (x = 0.10) as shown in Figure 4b. Numerous investigations have discussed thermal quenching behaviors.[16] They have explained thermal quenching by hole-trapping or electron transition. Although the thermal quenching behavior of phosphors has several determinants, the thermal degradation has not been discussed yet. To elucidate the thermal degradation of nitride phosphors, temperature-dependent emission peaks of $M_2Si_5N_8$ (M = Sr, Ba) were recorded from 25 to 300 °C (solid line) for heating and then from 300 to 25 °C (dashed line) for cooling under air, and the measured

intensities are plotted in the inset of Figure 4. Interestingly, the temperature-dependent emission spectra of the $Sr_{2-x}Si_5N_8$:Eu_x (x = 0.10) compound are irreversible, which also means thermal degradation. The intensity of the peak of $Sr_{2-x}Si_5N_8$:Eu_x (x = 0.10) from 300 to 25 °C was 55% of the value before heating up. The wavelength of emission peak, percentage of intensity, percentage of emission area, and full width at half-maximum (fwhm) are shown in Table 2. All

Table 2. Relative Emission Wavelength, Percentage of Intensity, Percentage of Emission Area, and Full Width at Half Maximum (fwhm) of Temperature-Dependent Luminescence Properties

$Sr_{2-x}Si_5N_8$:Eu_x (x = 0.02)			
temperature (°C)	wavelength (nm)	intensity (%)	fwhm (nm)
25/r25	606/606	100/100	77/77
50/r50	604/604	98/98	78/78
100/r100	604/604	94/94	80/80
150/r150	604/604	91/91	83/83
200/r200	602/602	87/87	85/85
250/r250	601/601	84/84	88/88
300	599	79	91
$Sr_{2-x}Si_5N_8$:Eu_x (x = 0.10)			
temperature (°C)	wavelength (nm)	intensity (%)	fwhm (nm)
25/r25	630/620	100/55	112/113
50/r50	626/624	96/54	115/117
100/r100	622/624	91/49	115/117
150/r150	614/614	84/44	115/117
200/r200	614/612	70/38	113/117
250/r250	610/612	48/32	117/117
300	606	25	116
$Ba_{2-x}Si_5N_8$:Eu_x (x = 0.10)			
temperature (°C)	wavelength (nm)	intensity (%)	fwhm (nm)
25/r25	622/622	100/100	123/123
50/r50	620/620	96/96	124/124
100/r100	618/618	88/88	125/124
150/r150	610/610	74/74	126/126
200/r200	606/606	54/54	125/125
250/r250	606/606	35/35	129/129
300	594	20	139

emission peaks are shifted to shorter wavelengths because of electron from the 5d band to the conduction band of the host-lattice, or from the 5d level to the 4f ground state via a crossing point. The Sr1 position has the loose site accommodating Eu^{2+} activators to correspond with a higher-energy (shorter-wavelength) emission peak, while the Sr2 position has the tight site accommodating Eu^{2+} activators to correspond with a lower-energy (longer-wavelength) emission peak.[17] The lower-energy (longer-wavelength) site has smaller activation energy to return to the ground state nonradiatively. As the temperature increases, the electron easily transfers from the 5d level to the 4f ground state via a crossing point through 8-coordination position. The reversible thermal behavior is called thermal quenching. However, the emission intensity of $Sr_{2-x}Si_5N_8$:Eu_x (x = 0.10) is irreversible when the sample is cooled to room temperature, and it was left to 55% of the initial intensity. The irreversible thermal behavior is called thermal degradation. In contrast, $Sr_{2-x}Si_5N_8$:Eu_x (x = 0.02) and $Ba_{2-x}Si_5N_8$:Eu_x (x = 0.10) are reversible, and the intensity of emission returns nearly to the same value at each degree during heating and cooling

processes. The possible mechanism for the thermal degradation of $Sr_{2-x}Si_5N_8:Eu_x$ ($x = 0.10$) is proposed to be due to the oxidation of the nitride host lattice or Eu^{2+} oxidized to Eu^{3+}.

To elucidate clearly the structural evolution upon heating treatment, we measured in situ X-ray diffraction during heating from 25 to 300 °C in air and cooling from 300 to 25 °C, as shown in Figure 5. During heating, no other peak was obtained
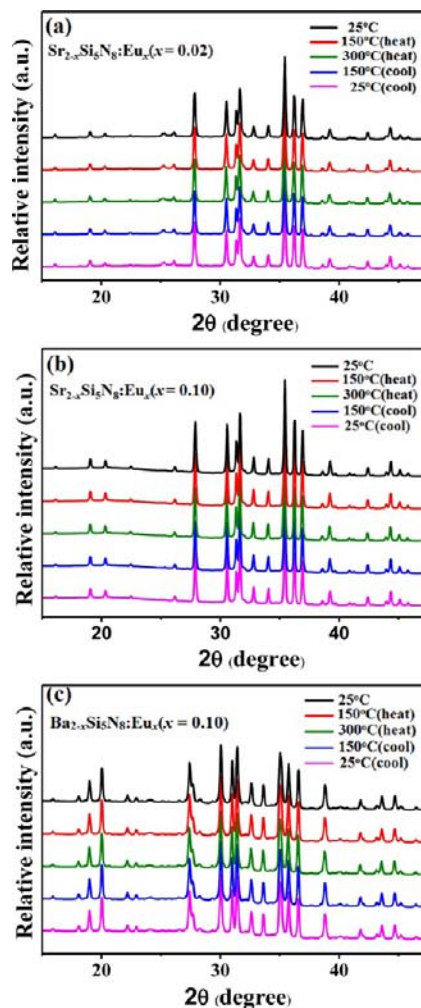

Figure 5. In situ XRD pattern of (a) $Sr_{2-x}Si_5N_8:Eu_x$ ($x = 0.02$), (b) $Sr_{2-x}Si_5N_8:Eu_x$ ($x = 0.10$), and (c) $Ba_{2-x}Si_5N_8:Eu_x$ ($x = 0.10$) samples.

from these three compounds. Because of thermal expansion, the XRD peaks are slightly shifted to lower angles as the temperature increases and returned to the same position as the sample is cooled back to room temperature. On the other hand, the relative intensity of the (122) plane is used to represent the whole variation of crystalline structure. It is due to the relative comparison; we choose the highest intensity of the 122 peak in $Sr_{2-x}Si_5N_8:Eu_x$ for the demonstration. The intensities of all peaks from the $Sr_{2-x}Si_5N_8:Eu_x$ ($x = 0.02$) and $Ba_{2-x}Si_5N_8:Eu_x$ ($x = 0.10$) samples (Figure 6a and c) vary reversibly, but those of the $Sr_{2-x}Si_5N_8:Eu_x$ ($x = 0.10$) samples decay to 95% of the initial intensity (Figure 6b). The characteristic of the $Sr_{2-x}Si_5N_8:Eu_x$ ($x = 0.10$) sample can also be speculated as that the crystallites partially decrystallized. Further detailed evolution of the crystal structure, obtained by in situ XRD measurements, is consistent with the temperature-dependent
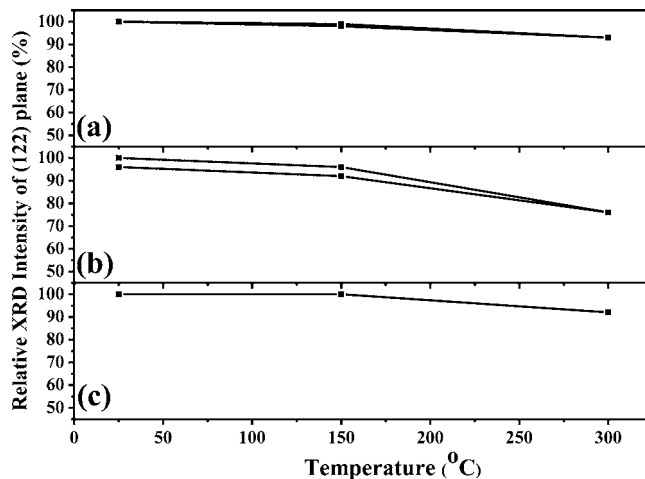

Figure 6. The relative intensity of the (112) peak of the XRD in situ pattern and unit cell volume of lattice (a) $Sr_{2-x}Si_5N_8:Eu_x$ ($x = 0.02$), (b) $Sr_{2-x}Si_5N_8:Eu_x$ ($x = 0.10$), and (c) $Ba_{2-x}Si_5N_8:Eu_x$ (Eu = 0.10) samples as a function of temperature.

luminescence spectra, revealing that the emission intensity decay is closely related to the structural collapse.

The reason for the degradation of the $Sr_{2-x}Si_5N_8:Eu_x$ ($x = 0.10$) sample after heating treatment in air is ascribed to formation of an amorphous layer (as observed by TEM in Figure 7). Figure 7a and c displays the transmission electron microscopic (TEM) images of $Sr_{2-x}Si_5N_8:Eu_x$ ($x = 0.10$) for as-prepared and heat-treated samples, respectively. The TEM images show the amorphous surface of the heat-treated $Sr_{2-x}Si_5N_8:Eu_x$ ($x = 0.10$) sample in air and a uniform crystallite size of around 100 nm. As shown in Figure 7b and d, the surface of the heat-treated $Sr_{2-x}Si_5N_8:Eu_x$ ($x = 0.10$) sample becomes amorphous. Therefore, it is speculated that the origin of thermal degradation of $Sr_{2-x}Si_5N_8:Eu_x$ ($x = 0.10$) is due to the formation of the amorphous phase.

The valence of the Eu ion is determined by the ESCA (electron spectroscopy for chemical analysis) measurements. Measurements were made of the as-prepared and heat-treated (at 300 °C in air) $Sr_{2-x}Si_5N_8:Eu_x$ ($x = 0.10$) compounds, and they were compared to those of the $Sr_{2-x}Si_5N_8:Eu_x$ ($x = 0.02$). ESCA analysis was conducted on the $Eu3d_{5/2}$ core level, as shown in Figure 8. On the basis of the shape and the energy position of the $Eu3d_{5/2}$ core level in the ESCA spectra of the Eu^{3+} and Eu^{2+} states of $Sr_{2-x}Si_5N_8:Eu_x$ compounds, the chemical state of Eu ions is clearly identified. Furthermore, the XANES analysis was used to determine the valence of Eu ions in Figure 9. The standard used in the XANES analysis of Eu^{3+} was Eu_2O_3, and that used in the analysis of Eu^{2+} was the commercial phosphor $BaMgAl_{10}O_{17}:Eu$ (BAM:Eu). The coexistence of Eu^{2+}/Eu^{3+} was observed in both XPS measurement and XANES analysis.

According to the ESCA measurements, the conversion of Eu^{3+} is higher than that of Eu^{2+} (independent of heating treatment), indicating that the material is oxidized at the surface resulting in conversion from Eu^{2+} to Eu^{3+} (ESCA is a surface-sensitive technique). This is in accordance with XANES measurements (a bulk-sensitive technique), which show a larger amount of Eu^{2+} as compared to Eu^{3+} in Figure 9 and listed in Table 3. For $Sr_2Si_5N_8:Eu$ ($x = 0.02$), a large amount of Eu^{3+} is already present before heat treatment in air, with roughly the same content after heating treatment. However, for
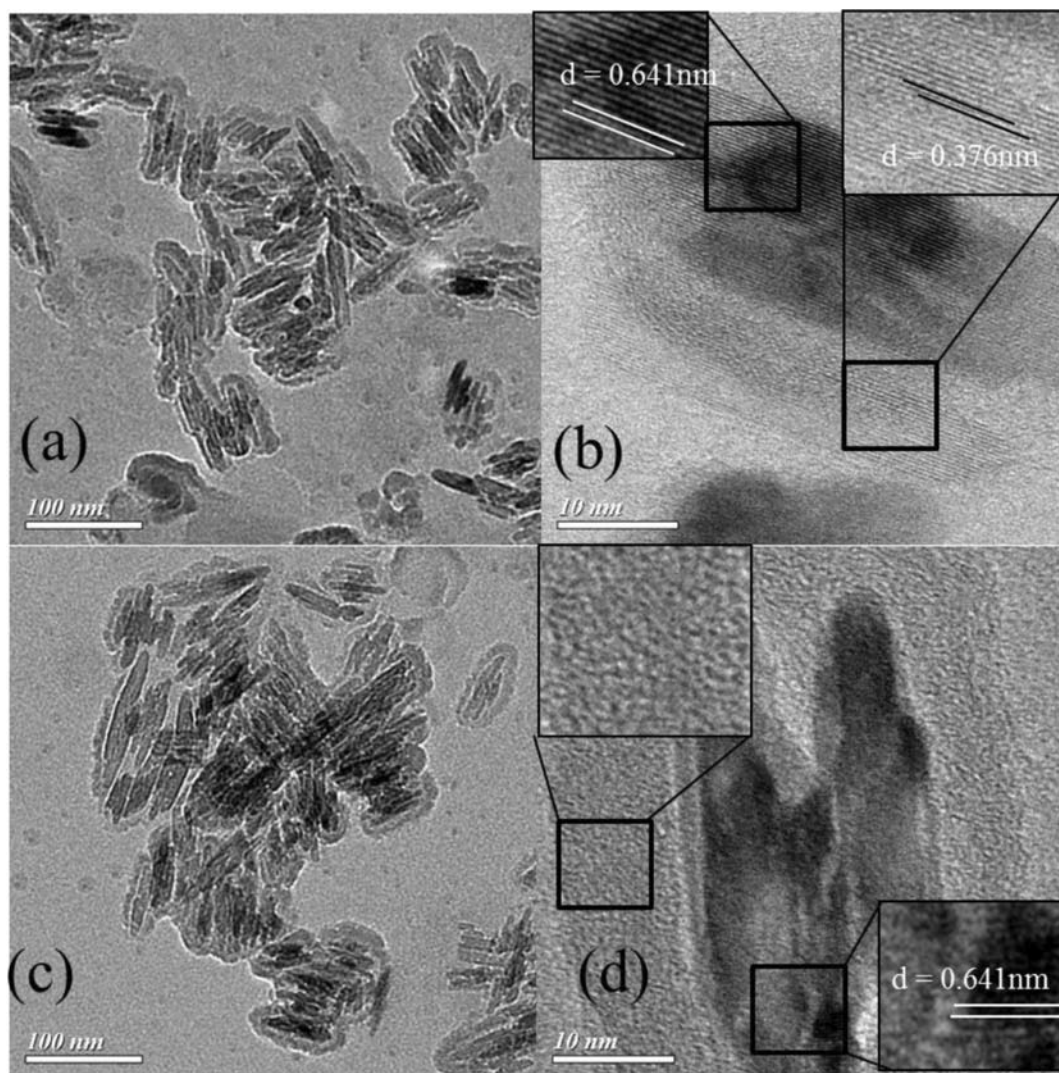
Figure 7. (a) TEM images and (b) HRTEM image of $Sr_{2-x}Si_5N_8:Eu_x$ ($x = 0.10$); and (c) TEM images and (d) HRTEM image of $Sr_{2-x}Si_5N_8:Eu_x$ ($x = 0.10$) after heating treatment at 300 °C.

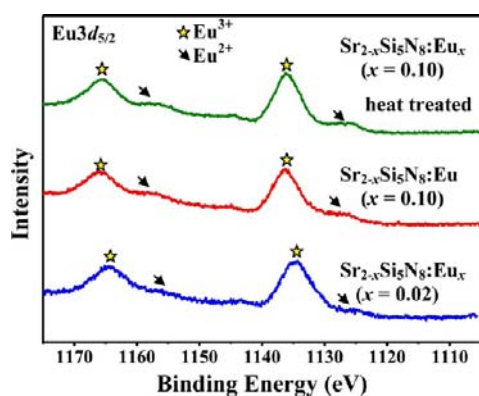**Figure 8.** ESCA spectra of the $Eu3d_{5/2}$ core level: (a) $Sr_{2-x}Si_5N_8:Eu_x$ ($x = 0.10$) after heating treatment at 300 °C, (b) fresh $Sr_{2-x}Si_5N_8:Eu_x$ ($x = 0.10$), and (c) $Sr_{2-x}Si_5N_8:Eu_x$ ($x = 0.02$) samples.

$Sr_2Si_5N_8:Eu$ ($x = 0.10$), the amount of Eu^{3+} increases after heating treatment. The contact of the $Sr_2Si_5N_8:Eu$ ($x = 0.10$) phosphor with the air will lead to oxidize Eu^{2+} to Eu^{3+} from the surface. So it seems that the thermal degradation of $Sr_2Si_5N_8:Eu$

is related to the increasing percentage of Eu^{3+} after heat treatment.

Comprehensively, the thermal degradation could be discussed and summarized by the following points. Oshio et al. identified that the presence of trivalent europium ions in $BaMgAl_{10}O_{17}:Eu^{2+}$ increases when the heating temperature of the heat treatment in air is increased.[19] The oxidation process for the electron transfer from dopant ions to adsorbed oxygen ions occurs when the divalent europium ions are close to adsorbed oxygen ions.[20] It corresponds with the XANES measurements. It is also found that the increased trivalent europium would make the surface amorphous. The amorphous phase could result in a decrease of the luminescence. For lower ($x = 0.02$) and higher ($x = 0.10$) Eu concentrations of $Sr_{2-x}Si_5N_8:Eu_x$ compounds, the degree of divalent europium ions oxidation depends on the probability of contact with oxygen in air which is higher for $x = 0.1$ than for $x = 0.02$, as illuminated in Scheme 1. To obtain further proof for the existence of oxygen in higher ($x = 0.10$) Eu concentration of $Sr_{2-x}Si_5N_8:Eu_x$ compounds, the O/N content for the samples is determined by ESCA analysis. The ESCA spectra in Figure 10 clearly confirm the results from before and after heating treatment $Sr_{2-x}Si_5N_8:Eu_x$ ($x = 0.10$) compounds. The wide
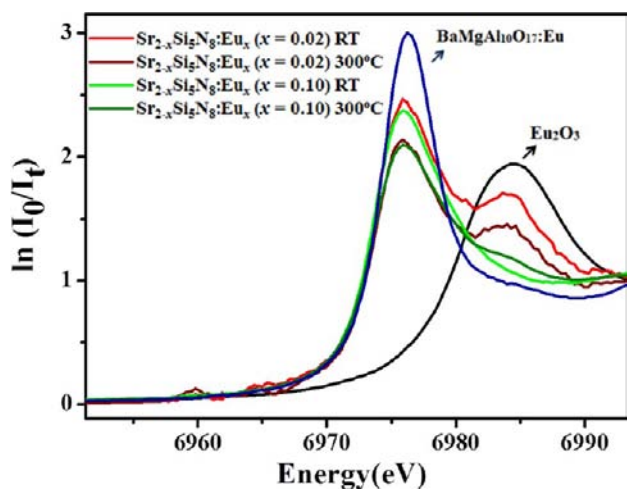
14114

dx.doi.org/10.1021/ja304754b | J. Am. Chem. Soc. 2012, 134, 14108−14117

Figure 9. The Eu L$_3$-edge XANES spectra for Sr$_{2-x}$Si$_5$N$_8$:Eu$_x$ (x = 0.02) at room temperature, Sr$_{2-x}$Si$_5$N$_8$:Eu$_x$ (x = 0.02) after 300 °C heat treatment in air, Sr$_{2-x}$Si$_5$N$_8$:Eu$_x$ (x = 0.10) at room temperature, and Sr$_{2-x}$Si$_5$N$_8$:Eu$_x$ (x = 0.02) after 300 °C heat treatment in air. The standards Eu$_2$O$_3$ for Eu^{3+} and commercial phosphor BaMgAl$_{10}$O$_{17}$:Eu (BAN:Eu) for Eu^{2+} are used as reference materials for XANES analysis.

Table 3. Intensity Ratio of Eu^{2+}:Eu^{3+} in Sr$_{2-x}$Si$_5$N$_8$:Eu$_x$ after Heating Treatment in Air at 300 °C by XANES Measurements

XANES measurements	intensity of Eu^{2+} (6976.255 eV)	intensity of Eu^{3+} (6984.654 eV)	ratio (Eu^{2+}:Eu^{3+})
Sr$_{2-x}$Si$_5$N$_8$:Eu$_x$ (x = 0.02)-room temperature	2.4377	1.6857	10:6.9
Sr$_{2-x}$Si$_5$N$_8$:Eu$_x$ (x = 0.02)-300	2.1102	1.4423	10:6.8
Sr$_{2-x}$Si$_5$N$_8$:Eu$_x$ (x = 0.10)-room temperature	2.3579	1.0560	10:4.4
Sr$_{2-x}$Si$_5$N$_8$:Eu$_x$ (x = 0.10)-300	2.0851	1.1632	10:5.5

Scheme 1. Sketch Showing the Ratio of Eu^{2+}/Eu^{3+} Is Decreased in Sr$_{2-x}$Si$_5$N$_8$:Eu$_x$ (x = 0.10) after 300 °C Heating Treatment in Air
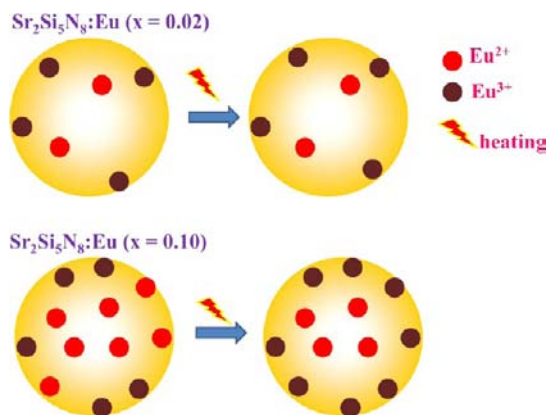
scan survey ESCA spectra are shown in Figure 10a. The detailed scan spectra of oxygen and nitrogen are shown in Figure 10b and c, respectively. The binding energy from 536 to 526 eV is assigned to the O 1s level and 402 to 392 eV is assigned to the N 1s level. The stronger signal of the oxygen peak in Sr$_{2-x}$Si$_5$N$_8$:Eu$_x$ (x = 0.10) compound could be
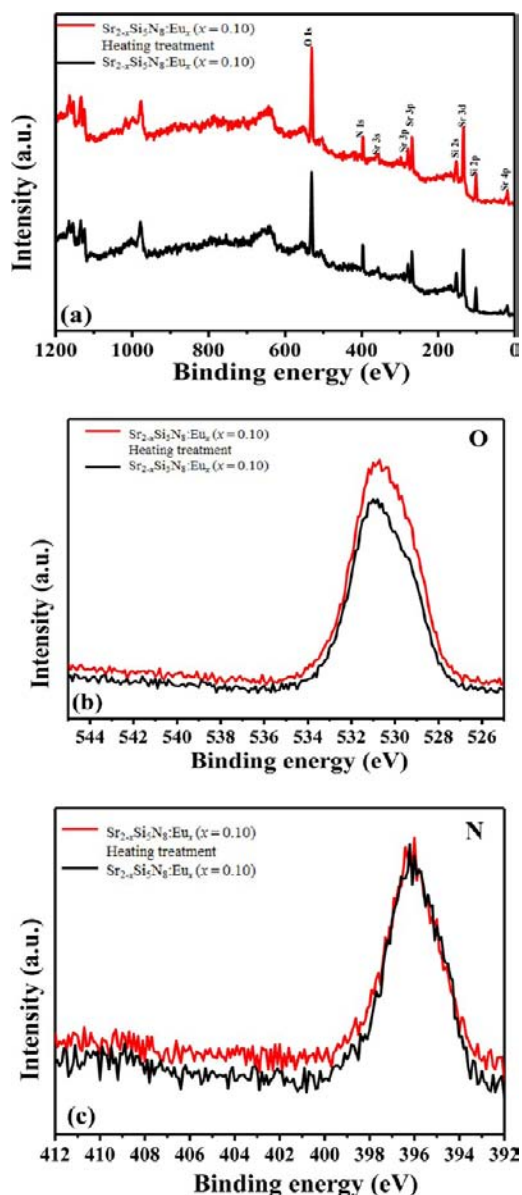

Figure 10. (a) Wide scan ESCA spectra of Sr$_{2-x}$Si$_5$N$_8$:Eu$_x$ (x = 0.10) and the sample after heating treatment in air. The detailed scan spectra of oxygen and nitrogen are shown in (b) and (c), respectively.

attributed to heating treatment. This additional oxygen in Sr$_{2-x}$Si$_5$N$_8$:Eu$_x$ (x = 0.10) after heating treatment led to a further oxidation process in Eu ion, as shown below.

The oxidation process is expressed by the following equation:[20]

$$2Eu^{2+} + \frac{1}{2}O_{2(g)} + V_N \rightarrow 2Eu^{3+} + O_N^{2-}$$
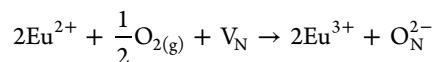
with V$_N$ an oxygen vacancy and O$_N^{2-}$ an oxygen. In this process, the mobility of the Eu^{2+} ion is of importance. The heating process makes the oxygen flow more quickly, or an increase in the mobility of oxygen diffusing into the lattice and the oxidation process occurs likely at the surface of phosphors.

In Sr$_{2-x}$Si$_5$N$_8$:Eu$_x$ compounds, the covalence of Sr−N is higher than that of Sr−O, which makes the Eu^{2+} have a higher probability to connect with oxygen. In higher (x = 0.10) Eu concentration of Sr$_{2-x}$Si$_5$N$_8$:Eu$_x$ compound, the thermal degradation would occur obviously. In Ba$_{2-x}$Si$_5$N$_8$:Eu$_x$ com-

pounds, the covalency of Ba−N is not as high as Sr−N, which make the Ba have a higher probability to connect with nitrogen. On the basis of the points mentioned above, the mechanism of thermal degradation in the $M_2Si_5N_8:Eu_x$ (M = Sr or Ba) system is elucidated in Scheme 2.

Scheme 2. Sketch Showing the Covalence in Sr_2Si_5N8 and $Ba_2Si_5N_8$ Compounds of Two Different Types
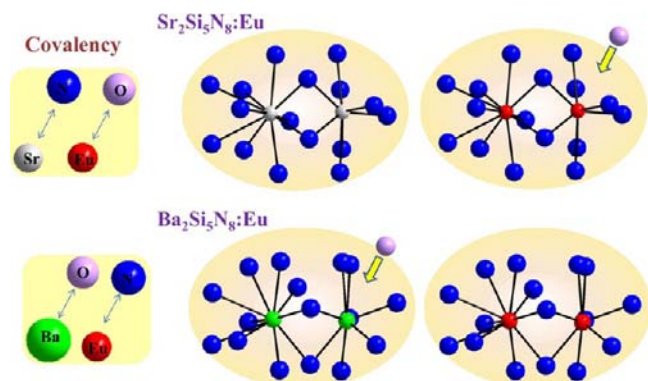
CONCLUSION

In summary, a simple solid-state route was adopted to fabricate a series of nitridosilicate phosphors compounds, $M_{2−x}Si_5N_8:Eu_x$ (M = Sr, Ba). With respect to the temperature dependence of the emission properties of $M_{2−x}Si_5N_8:Eu_x$ (M = Sr, Ba), we clearly demonstrate the thermal degradation of phosphors after heating to 300 °C in air. In situ XRD patterns clearly indicate the variation of crystallinity upon heating. On the basis of in situ XRD measurements, the structure decomposes at the surface upon heating treatment. According to ESCA and XANES analysis, the large amounts of Eu^{2+} converted to Eu^{3+} are a key reason for thermal degradation. The morphology of these materials was examined by TEM technique. From the XANES analysis, in situ XRD measurements, and TEM image, the mechanisms of the $M_2Si_5N_8:Eu_x$ (M = Sr, Ba) system could be concluded by the following rule: the charge transfer readily occurs from dopant ions to oxygen ions when divalent europium ions are close to the oxygen ions in the $Sr_{2−x}Si_5N_8:Eu_x$ compound. The thermal degradation of $Sr_{2−x}Si_5N_8:Eu_x$ (x = 0.10) is proposed to be due to oxidation of the nitride host lattice or Eu^{2+} oxidized to Eu^{3+}. It also points out that the covalence of Sr−N being higher than that of Ba−N causes the oxygen to easily change the Eu^{2+} to Eu^{3+} in the $Sr_{2−x}Si_5N_8:Eu_x$ (x = 0.10) sample.

AUTHOR INFORMATION

Corresponding Author
rsliu@ntu.edu.tw
Notes
The authors declare no competing financial interest.

ACKNOWLEDGMENTS

REFERENCES

(1) (a) Nakamura, S.; Mukai, T.; Senoh, M. *Appl. Phys. Lett.* **1994**, *64*, 1687. (b) Schubert, E. F.; Kim, J. K. *Science* **2005**, *308*, 1274. (c) Ki, W.; Li, J. *J. Am. Chem. Soc.* **2008**, *130*, 8114.

(2) (a) Jang, H. S.; Im, W. B.; Lee, D. C.; Jeon, D. Y.; Kim, S. S. *J. Lumin.* **2007**, *126*, 371. (b) Chen, Y.; Gong, M.; Wang, G.; Su, Q. *Appl. Phys. Lett.* **2007**, *91*, 071117.

(3) Li, Y. Q.; De With, G.; Hintzen, H. T. *J. Solid State Chem.* **2008**, *181*, 515.

(4) (a) Xie, R. J.; Hirosaki, N. *Sci. Technol. Adv. Mater.* **2007**, *8*, 588. (b) Li, Y. Q.; De With, G.; Hintzen, H. T. *J. Lumin.* **2006**, *116*, 107. (c) Liu, R. S.; Liu, Y. H.; Bagkar, N. C.; Hu, S. F. *Appl. Phys. Lett.* **2007**, *91*, 061119. (d) Bachmann, V.; Ronda, C.; Oeckler, O.; Schnick, W.; Meijerink, A. *Chem. Mater.* **2009**, *21*, 316.

(5) (a) Hintzen, H. T.; Van Krevel, J. W. H.; Botty, G. Patent EP 1104799 20010606. (b) Van Krevel, J. W. H. Ph.D. Thesis, Eindhoven University of Technology, 2000.

(6) Lin, M. T.; Tai, K. Y. *Materialsnet* **2009**, *3*, 80.

(7) (a) Piao, X.; Horikawa, T.; Hanzawa, H.; Machida, K. *Appl. Phys. Lett.* **2006**, *88*, 161908. (b) Bol, A. A.; Meijerink, A. *Phys. Chem. Chem. Phys.* **2001**, *3*, 2105. (c) Kurushima, T.; Gundiah, G.; Shimomura, Y.; Mikami, M.; Kijima, N.; Cheetham, A. K. *J. Electrochem. Soc.* **2010**, *157*, J64. (d) Pratt, S. T. *Annu. Rev. Phys. Chem.* **2005**, *56*, 281.

(8) (a) Xie, R. J.; Hirosaki, N.; Suehiro, T.; Xu, F. F.; Mitomo, M. *Chem. Mater.* **2006**, *18*, 5578. (b) Zeuner, M.; Schmidt, P. J.; Schnick, W. *Chem. Mater.* **2009**, *21*, 2467. (c) Zeuner, M.; Hintze, F.; Schnick, W. *Chem. Mater.* **2009**, *21*, 336. (d) Duan, C. J.; Wang, X. J.; Otten, W. M.; Delsing, A. C. A.; Zhao, J. T.; Hintzen, H. T. *Chem. Mater.* **2008**, *20*, 1597.

(9) Larson, C. Von Dreele, R. B. Generalized Structure Analysis System(GSAS). *Los Alamos National Laboratory Report LAUR 86-748*; Los Alamos National Laboratory: Los Alamos, NM, 1994.

(10) Schlieper, T.; Milius, W.; Schnick, W. *Z. Anorg. Allg. Chem.* **1995**, *621*, 1380.

(11) Shannon, R. D. *Acta Crystallogr.* **1976**, *A32*, 751.

(12) (a) Zhang, Q. H.; Wang, J.; Yeh, C. W.; Ke, W. C.; Liu, R. S.; Tang, J. K.; Xie, M. B.; Liang, H. B.; Su, Q. *Acta Mater.* **2010**, *58*, 6728. (b) Chan, T. S.; Liu, R. S.; Baginskiy, I. *Chem. Mater.* **2008**, *20*, 1215. (c) Ganguly, P.; Shah, N.; Phadke, M.; Ramaswamy, V.; Mulla, I. S. *Phys. Rev. B* **1993**, *47*, 991.

(13) (a) Li, Y. Q.; De With, G.; Hintzen, H. T. *J. Solid State Chem.* **2008**, *181*, 751. (b) Zeuner, M.; Pagano, S.; Schnick, W. *Angew. Chem., Int. Ed.* **2011**, *50*, 7754.

(14) (a) Clarke, S. J.; DiSalvo, F. J. *Inorg. Chem.* **1997**, *36*, 1143. (b) Hecht, C.; Stadler, F.; Schmidt, P. J.; Schmedt auf der Günne, J.; Baumann, V.; Schnick, W. *Chem. Mater.* **2009**, *21*, 1595. (c) Kechele, J. A.; Hecht, C.; Oeckler, O.; Schmedt auf der Günne, J.; Schmidt, P. J.; Schnick, W. *Chem. Mater.* **2009**, *21*, 1288. (d) Brunner, G. O.; Meier, W. M. *Nature* **1989**, *337*, 146. (e) Shibata, N.; Pennycook, S. J.; Gosnell, T. R.; Painter, G. S.; Shelton, W. A.; Becher, P. F. *Nature* **2004**, *428*, 730.

(15) (a) Li, Y. Q.; Van Steen, J. E. J.; Van Krevel, J. W. H.; Botty, G.; Delsing, A. C. A.; DiSalvo, F. J.; De With, G.; Hintzen, H. T. *J. Alloys Compd.* **2006**, *417*, 273. (b) Li, Y. Q.; Delsing, A. C. A.; De With, G.; Hintzen, H. T. *Chem. Mater.* **2005**, *17*, 3242.

(16) (a) Lin, C. C.; Xiao, Z. R.; Guo, G. Y.; Chan, T. S.; Liu, R. S. *J. Am. Chem. Soc.* **2008**, *43*, 5659. (b) Piao, X.; Machida, K.; Horikawa, T.; Hanzawa, H.; Shimomura, Y.; Kijima, N. *Chem. Mater.* **2007**, *19*, 4592. (c) Li, Y. Q.; Hirosaki, N.; Xie, R. J.; Takeda, T.; Mitomo, M. *Chem. Mater.* **2008**, *20*, 6704. (d) Liu, W.-R.; Yeh, C.-W.; Huang, C.-H.; Lin, C. C.; Chiu, Y.-C.; Yeh, Y.-T.; Liu, R.-S. *J. Mater. Chem.* **2011**, *21*, 3740. (e) Piao, X.; Horikawa, T.; Hanzawa, H.; Machida, K. *J. Electrochem. Soc.* **2006**, *153*, H232.

(17) (a) Dorenbos, P. *Phys. Rev. B* **2000**, 15650. (b) Dorenbos, P. *Phys. Rev. B* **2000**, *62*, 15640. (c) Dorenbos, P. *Phys. Rev. B* **2001**, *64*, 125117. (d) Sohn, K.-S.; Lee, B.; Xie, R.-J.; Hirosaki, N. *Opt. Lett.* **2009**, *34*, 3427. (e) Sohn, K. S.; Lee, S. J.; Xie, R. J.; Hirosaki, N. *Appl. Phys. Lett.* **2009**, *95*, 121903.

(18) Ziegler, A.; Idrobo, J. C.; Cinibulk, M. K.; Kisielowski, C.; Browning, N. D.; Ritchie, R. O. *Science* **2004**, *306*, 1768.

(19) Oshio, S.; Matsuoka, T.; Tanaka, S.; Kobayashi, H. *J. Electrochem. Soc.* **1998**, *145*, 3903.

(20) Bizarri, G.; Moine, B. *J. Lumin.* **2005**, *113*, 199.

14117

dx.doi.org/10.1021/ja304754b | *J. Am. Chem. Soc.* 2012, 134, 14108−14117